Journal of Fluids and Structures (2002) **16**(2), 123–136
doi:10.1006/jfls.2001.0406, available online at http://www.idealibrary.com on IDEAL®

DYNAMICS OF AN IN-LINE TUBE ARRAY SUBJECTED TO STEAM–WATER CROSS-FLOW. PART I: TWO-PHASE DAMPING AND ADDED MASS

T. Nakamura, K. Hirota and Y. Watanabe

Mitsubishi Heavy Industries, Ltd., Takasago R&D Center, 2-1-1 Arai-cho, Shinhama Takasago, Hyogo, Japan

N. W. Mureithi

Department of Mechanical Engineering, Kobe University, Rokkodai 1-1 Nada-ku, Kobe, Japan

T. Kusakabe

Mitsubishi Heavy Industries, Ltd., Kobe Shipyard and Machinery Works 1-1 Wadasaki-cho 1-chome, Hyogo-ku, Kobe, Japan

AND

H. Takamatsu

The Kansai Electric Power Co., Inc. 3-3-22, Nakanoshima, Kita-ku, Osaka, Japan

(Received 28 October 1999, and in final form 22 May 2001)

We report the results of a recent MHI study in which three important aspects of fluidelastic instability were considered: (i) two-phase fluid damping and added mass under prototypical conditions, (ii) the nature of unsteady fluid forces leading to fluidelastic instability, and finally (iii) the fluidelastic instability mechanism itself. This paper is the first in a three-part series reporting on the findings of the comprehensive study. Tests have been conducted to determine two-phase flow damping under prototypical high temperature and pressure conditions, up to 5·8 MPa at 273°C. The test array was of an in-line geometry. Two separate arrays were tested, a standard configuration with flow normal to the tube axis and an array inclined at 30° to the flow. Measurements were conducted for various pressures (and correspondingly temperatures), void fractions, phase flow velocities as well as tube location within the array. Damping was nominally higher for the inclined array. Tubes at the array extremities were found to experience the highest damping levels. This is attributed to entrance and exit effects. A distinct difference between drag- and lift-direction damping was observed. Tube added mass showed a quasilinear variation with void fraction. Added mass values were found to vary significantly from computed values assuming homogeneous fluid properties.

1. INTRODUCTION

There has been significant progress made in understanding the basic mechanisms underlying fluidelastic instability in tube arrays, particularly for single-phase flow. Less well understood are the mechanisms involved when two fluid phases are present.

As first shown by Pettigrew & Gorman (1981) and later by others (Axisa *et al.* 1985; Pettigrew *et al.* 1985; Nakamura *et al.* 1995), fluidelastic instability may also occur in two-phase flow.

0889–9746/02/020123 + 14 $35.00/0

Damping is possibly the most important parameter in stability evaluation of tube arrays. A multiplicity of parameters come into play for two-phase flow. Carlucci (1980), and later Pettigrew & Knowles (1992), suggested the inclusion of an additional two-phase damping component. Carlucci & Brown (1983) postulated that two-phase damping was the result of a detuning process caused by temporal variation in the tube hydrodynamic mass. Two-phase damping is known to depend on void fraction, surface tension, frequency, hydrodynamic mass-to-tube mass ratio, etc. [see Pettigrew & Knowles (1992)]. The relation between damping and these parameters is only partially understood—with the exception perhaps, of the void fraction dependence.

Some pioneering work by Hara & Kohgo (1986) and Hara (1993) has provided some useful insights into the two-phase damping generating mechanisms. However, the potential for a theoretical analysis to predict two-phase damping remains rather limited.

For design application, experimental measurements remain invaluable for accumulating data on two-phase damping. There is at present a limited amount of data on two-phase damping, particularly under prototypical steam generator operating conditions. Notably, the data by Axisa *et al.* (1984, 1985, 1986, 1988) remain by far the most comprehensive. Their measurements indicated that damping shows a clear decrease with steam quality. Damping in the drag direction was found to be higher than in the lift direction. Air–water and steam–water mixtures displayed the same trends in damping variation, albeit with different magnitudes; up to 50% higher for air–water. The latter raises questions as to the validity of applying air–water data to actual designs.

Pettigrew & Knowles (1992) investigated in some detail the effect of various parameters on two-phase damping, including void fraction, surface tension, frequency and confinement. Tests were conducted using air–water two-phase mixtures. The effect of void fraction was found to be dominant. Maximum damping varied between 2 and 4%, depending on surface tension. The correlation to surface tension was fairly complex and depended on excitation frequency, indicating that frequency and surface tension effects were coupled. In general, damping increased with surface tension.

The work presented in this paper provides additional two-phase data, as well as some insights deriving from a careful study of the experimental results. Most importantly, the data correspond to prototypical high temperature and pressure conditions.

New damping measurement and analysis techniques which we believe to be more accurate were developed and employed in this test program. Damping was measured under several high pressure and temperature conditions, covering both homogeneous and non-homogeneous flow regimes. This paper is the first in a three-part series. Unsteady fluid forces and stability measurement and analysis are presented in Mureithi *et al.* (2002) and Hirota *et al.* (2002), respectively. The main aspects of this work were previously reported in the series Nakamura *et al.* (1996), Mureithi *et al.* (1996) and Hirota *et al.* (1996).

2. TEST APPARATUS AND PROCEDURE

Figure 1 shows the test loop and array geometry. The U-tube heat exchanger (below the test section) rated 2 MW, can generate steam–water two-phase flow at a maximum pressure of 6 MPa and temperature 273°C. The mixture flows upwards against gravity as cross-flow through the array. Steam and water flow rates can be measured at the respective outlets. The maximum average steam flow rate varies from 4·5 to 12 m/s depending on pressure (temperature). The liquid velocity range is 0–1·0 m/s. Void fraction values from 0·5 to 1·0 can be attained.

The test array is depicted in Figure 1(b). It consists of 30 tube rows with five tubes per row. Tube diameter is 22·23 mm and array pitch is 32·54 mm. The 161-mm-long tubes

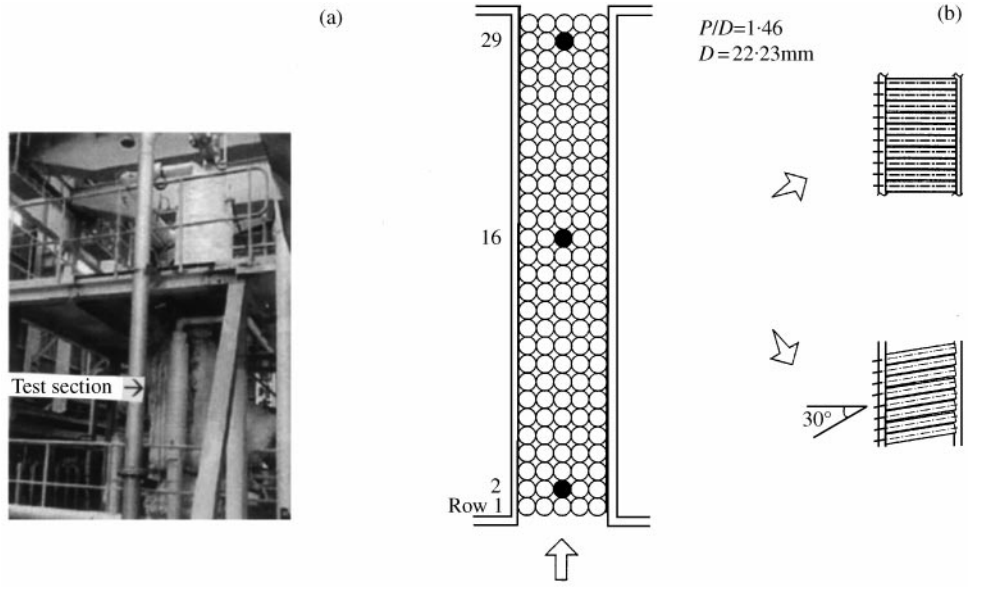

Figure 1. (a) Partial view of test loop and (b) array geometry.

(horizontal configuration) are all essentially rigidly fixed, with the exception of three tubes. In the second type of configuration, tubes are inclined 30°; the projected length, normal to the flow, was 161 mm. The centrally located tubes in rows 2, 16 and 29 are supported using flexible rods as detailed in Figure 2(a). These flexibly mounted tubes have a mass of 0·96 kg/m.

To counter thermal expansion effects a rather complex support structure is necessary. With one end rigidly fixed, the other is fitted with a linear bearing which allows for thermal expansion, the resulting slack being taken up by a preloaded spring, see Figure 2(a). Figure 2(b) shows an overview of the assembled array within the test-section. Figure 2(c, d) shows photographs of part of the test-section and a close-up view of a removable tube bundle containing a flexible tube.

In these tests, damping could be measured in either a *passive* or *active* mode. In the former case, fluid random excitation results in tube response from which damping can be determined, assuming a flat turbulence excitation spectrum in a band centred at the tube natural frequency. In the latter case, an independent mechanism produces the tube excitation. The mechanism comprises an electromagnet and a target block mounted on the support wire, Figure 2; the actual system comprises two pairs of magnets, one each for the lift and drag directions. Figure 2(d) shows an external view of the system.

The tubes were excited in one of two ways. To obtain free decay traces, excitation at the resonance frequency was cut off after several seconds of steady-state vibration. The second type of test involved sweep excitation. Both a flat excitation spectrum and controlled response amplitude could be achieved in this case.

Tests were conducted at four pressure levels, 0·1 (single phase only), 0·5, 3·0 and 5·8 MPa. The single-phase flow test, being a reference and equipment verification case, is not presented here. For the high pressures, the pressure drop across the tube array is small. At the highest pressure, measurements were made for void fractions in the range 0·70–0·96. Thermal-hydraulic tests conducted simultaneously with vibration tests indicated the following flow patterns: 0·5 MPa, intermittent flow; 3·0 and 5·8 MPa, homogeneous froth flow.

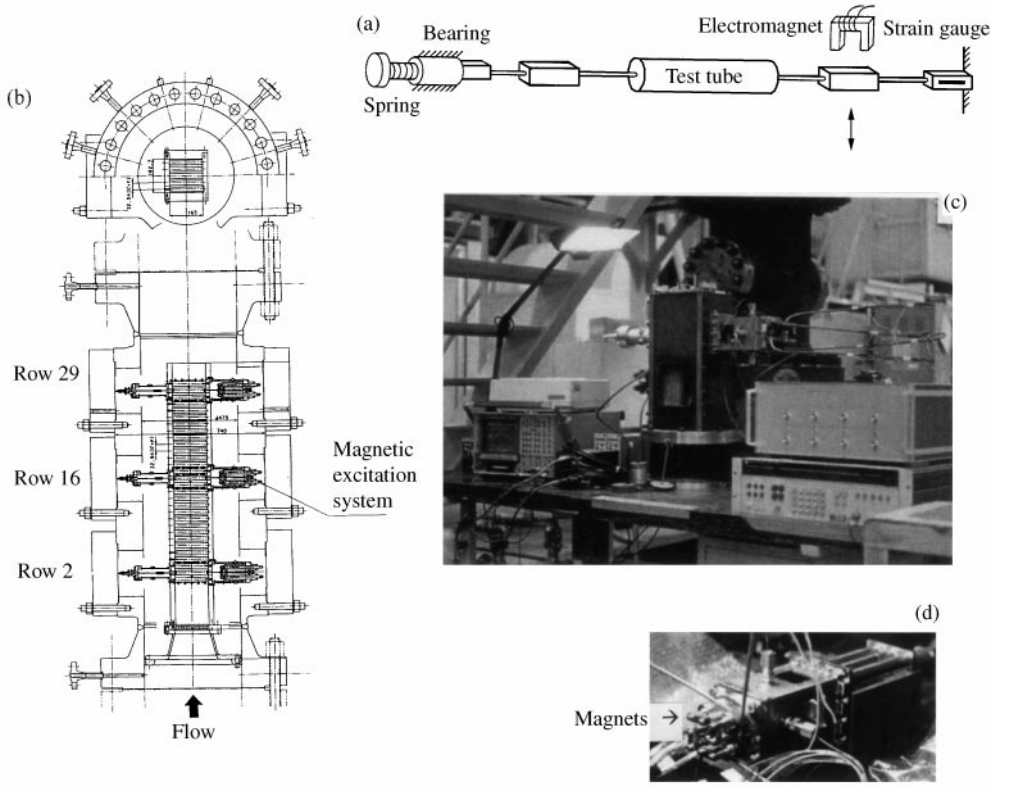

Figure 2. (a) Schematic of measurement tube; (b) view of array in test-section; (c, d) assembled tube bundles (in the vicinity of the test tube) showing (c) part of test-section with the removable bundle including test cylinder, and (d) close-up view of removable bundle.

The average void fraction was found to be independent of row depth. Thermal hydraulic tests and results are detailed in Appendix A.

3. DATA REDUCTION AND DEFINITION OF PARAMETERS

3.1. Data Processing and Reduction

Improved data analysis was an important consideration in this study. For real-time on-line monitoring, a Hilbert transform analysis proved far superior to the standard logarithmic decrement method. Post-processing was done using time-domain identification (Mureithi *et al.* 1995).

Damping and natural frequencies in air and water, at atmospheric conditions, are given in Table 1 for the three test tubes. In this and subsequent figures, test tubes are identified by the letter S followed by the row number. Lift and drag directions are distinguished by the letters L and D, respectively; hence S2D, for instance, refers to the drag direction of the second row tube.

3.2. Definition of Parameters

Average quantities based on an assumption of homogeneous two-phase flow are used throughout the paper unless otherwise specified. The superficial liquid and gas

TABLE 1

Test tube frequency and damping at atmospheric conditions

Tube and direction	Air		Water ($P = 0{\cdot}1$ MPa, 20°C)		
	Frequency (Hz)	Damping (ζ_s%)	Frequency (Hz)	Damping	
				Total (ζ_t%)	Flow-induced ($\zeta = \zeta_t - \zeta_s$)%
S29D	21·7	0·29	17·6	0·91	0·63
S29L	21·8	0·30	17·7	0·91	0·62
S16D	22·0	0·32	17·8	0·91	0·59
S16L	22·1	0·40	17·9	0·98	0·59
S2D	21·8	0·40	17·6	1·04	0·65
S2L	21·8	0·45	17·5	1·14	0·69

gap velocities j_l and j_g are defined as

$$j_l = \frac{W_l}{\rho_l A}, \qquad j_g = \frac{W_g}{\rho_g A}, \tag{1}$$

where W_l and W_g are the corresponding mass flow rates, ρ_l and ρ_g the fluid densities, and A the total gap cross-section area. The superficial void fraction β is then defined as

$$\beta = \frac{j_g}{j_g + j_l}. \tag{2a}$$

A homogeneous density $\rho = \rho_g\beta + \rho_l(1 - \beta)$ may then be defined. Using j_g and j_l, an average flow velocity U is defined as

$$U = j_g + j_l. \tag{2b}$$

Fluid damping is determined by subtracting the structural damping ζ_s from total measured damping (ζ_t). Therefore total fluid damping ζ is: viscous (ζ_v) + flow-dependent (ζ_{fd}) + two-phase damping (ζ_{tp}), or

$$\zeta = \zeta_v + \zeta_{fd} + \zeta_{tp} = \zeta_t - \zeta_s. \tag{3}$$

Carlucci (1980) proposed the formulation of equation (3).

3.3. REDUCTION PROCEDURE FOR RAW DATA

A typical transfer function [or frequency response function (FRF)] and free decay trace for the row 16 tube (S16) vibrating in the drag direction are shown in Figure 3. These are for pressure $P = 5{\cdot}8$ MPa (temperature 273°C), $j_l = 0{\cdot}21$ m/s, and $j_g = 1{\cdot}9$ m/s (hence $\beta = 0{\cdot}9$).

Damping from the transfer function could be determined either by direct curve fitting on the transfer function or by complex exponentials in time domain (Mureithi *et al.* 1995) applied to the corresponding impulse response function. The latter method was also applied to the free decay time traces. To average out transient effects in the free decay data, a weighted averaging procedure was used. Thus,

$$\zeta = \tfrac{1}{2}[\zeta_{\text{sweep}} + 0{\cdot}5(\zeta_{fd1} + \zeta_{fd2})], \tag{4}$$

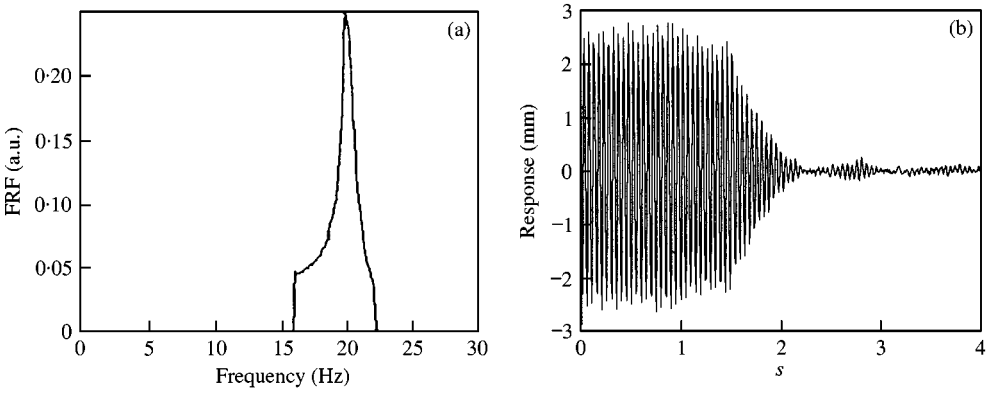

Figure 3. Sample raw data for the drag direction: (a) sweep test frequency response function (FRF); (b) transient response time trace.

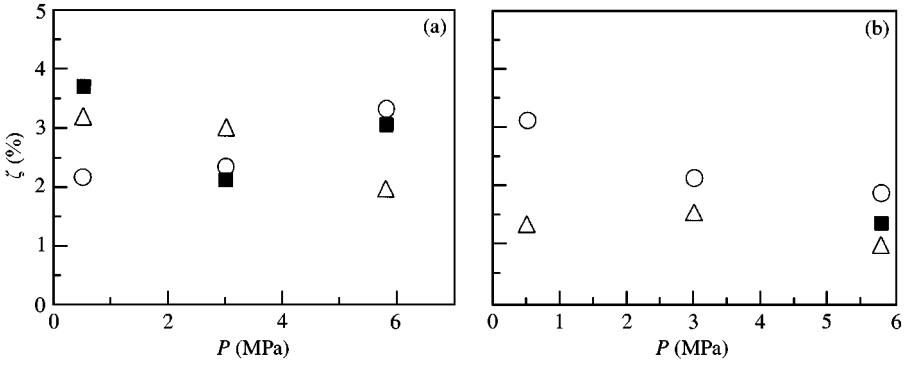

Figure 4. Average damping for $P = 0{\cdot}5$, 3·0, 5·8 MPa and $U = 1{\cdot}33$ m/s; $\beta = 0{\cdot}90$: (a) drag; (b) lift. Data shown are for tube: ■, S2; △, S16; and ○, S29.

where ζ_{sweep} is damping obtained via a sweep test, and ζ_{fd1} and ζ_{fd2} are damping values from two consecutive free decay tests.

The test tubes were excited with a nominal peak amplitude in the range 1·5–2·5 mm, (0·07D–0·11D).

4. RESULTS AND DISCUSSION

4.1. Variation of Damping for $\beta = 0{\cdot}90$ and $P = 0{\cdot}5$, 3·0, 5·8 MPa

In the results presented in the figures, the averaged total fluid damping, ζ, as defined in equation (3), is presented; (the only exception is Figure 8 where an estimate of the two-phase damping component, ζ_{tp}, is presented).

Figure 4 shows average damping at $U(= j_g + j_l) = 1{\cdot}33$ m/s for the lift and drag directions for the horizontal array for $P = 0{\cdot}5$, 3·0 and 5·8 MPa. The average drag direction damping is 2·7% at all three pressures. In the lift direction, the average damping is essentially unchanged for tube S16, but decreases between 0·5 and 3·0 MPa pressure for tube S29.

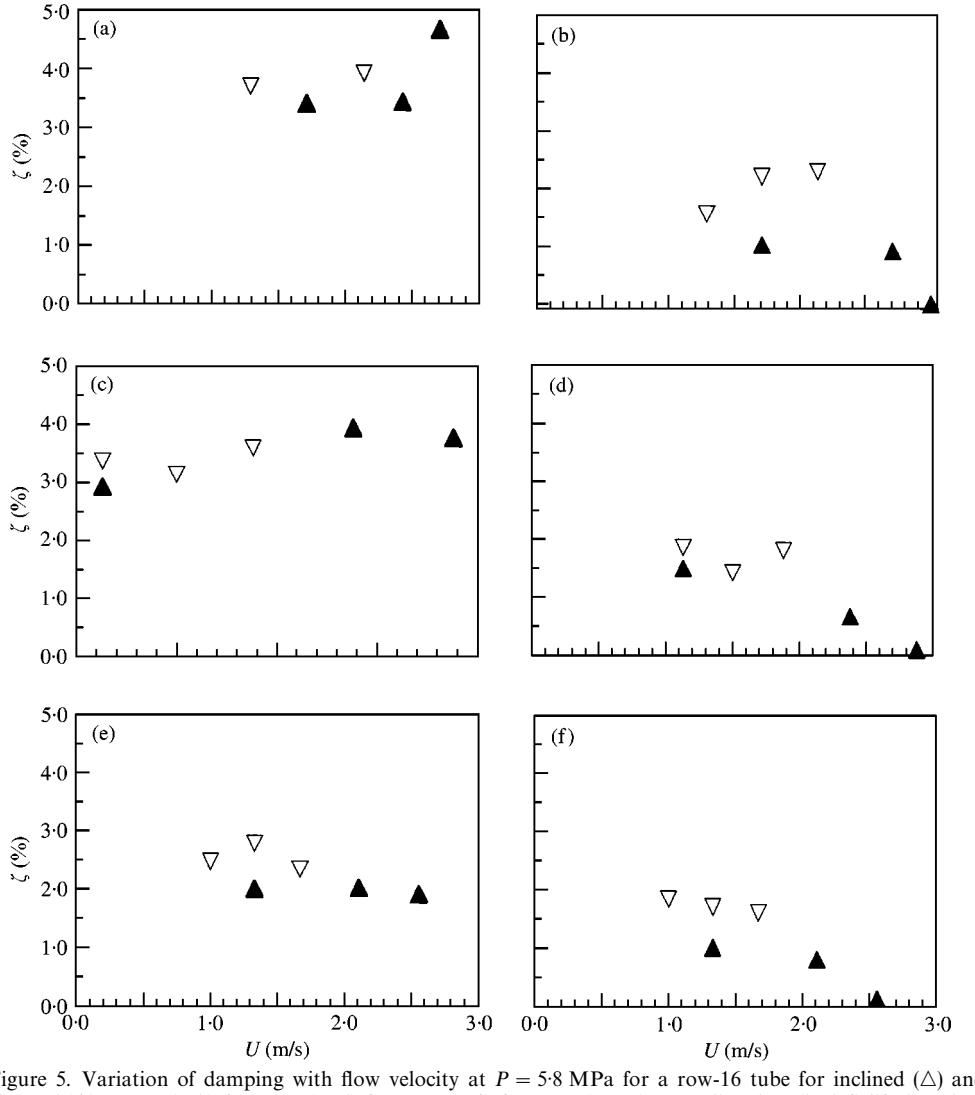

Figure 5. Variation of damping with flow velocity at $P = 5{\cdot}8$ MPa for a row-16 tube for inclined (△) and horizontal (▲) arrays: (a, b) $\beta = 0{\cdot}70$; (c, d) $\beta = 0{\cdot}80$; (e, f) $\beta = 0{\cdot}90$. (a, c, e) Drag direction; (b, d, f) lift direction.

4.2. Damping Variation with Flow Velocity and Void Fraction

Figure 5 shows the variation of ζ with U at 5·8 MPa. Data for both arrays at $\beta = 0{\cdot}7$, 0·8 and 0·9 are shown. The effect of variation of the flow-dependent damping component [ζ_{fd} in equation (3)] is apparent at the higher flow velocities. A large decrease in lift-direction damping occurs; although not shown, this is also the case for $P = 3{\cdot}0$ MPa. This is the fluidelastically unstable direction. For both arrays, drag-direction damping is clearly higher than its lift-direction counterpart even at velocities well below the instability velocity. The critical velocity U_c is approximately 2·1 m/s for tube S16 [see Part III, Hirota *et al.* (2002)]. In general, damping was found to be marginally higher for the inclined array.

4.3. Two-Phase Damping and Comparison with Existing Data

Fluidelastic instability ($U = U_c$) occurs when the flow-dependent damping becomes negative to the point where the net effective damping is zero. With reference to equation (3), this

condition may be expressed as $-\zeta_{fd} = \zeta_{tp} + \zeta_v + \zeta_s \Rightarrow U = U_c$. We assume that ζ_{fd} is initially zero (at zero and low flow velocities). The net positive damping ($\zeta + \zeta_s$) then gives us a measure of the "stability" of the tube in the fluid; thus, the higher $\zeta + \zeta_s$ is, the more stable the tube. Data in Part III of this series (Hirota *et al.* 2002) support this assertion. Ideally, the value of ζ at zero flow should be used. Since this is not possible, the damping at velocities well below the fluidelastic instability threshold is used instead. The limiting velocity was judged from instability data (Hirota *et al.* 2002) and was on average about 50% of the instability velocity. Average damping and standard deviations were calculated for each void fraction considering all the tubes; i.e., the effect of tube position within the array is not considered in this case. For the horizontal array, damping results for varying void fraction are combined in Figure 6. This figure contains selected data, all at low velocities, below 50% of the instability velocity. For each void fraction, an average of five data were available. These appear in the figure. The average value (over all tubes) for each void fraction is shown by open circles; the associated variance is also indicated. As the void fraction increases, the overall damping decreases. This variation is more apparent in the drag direction, due to the wider range over which damping changes. The tubes located at the extremities (rows 2 and 29) show the largest variance in damping at a given void fraction. Damping in row 16 tends to be lower and with less variance than at the two extreme locations. The error bars in the graphs show the range of the data for two standard deviations from the mean value.

The centrally located S16 tube is considered to be the most practically representative from a design point of view. For both tube arrays, final averaged data for tube S16 are presented in Figure 7. In the figures the solid line is a least-squares second-order fit of the averaged data; the broken lines show the two standard deviations statistical bounds, where σ_b is the average standard deviation over all β for the horizontal array. For the horizontal array the averaged data shows the typical parabolic-like variation of ζ with β. Values of ζ showed larger variance for the inclined array, especially at lower values of β.

In order to compare the present data with the results of Axisa *et al.* (1984, 1985, 1986, 1988), viscous and flow–drag-dependent damping expressions employed by Axisa *et al.* were used to reduce the present data to an equivalent two-phase damping ζ_{tp}. Viscous (ζ_v) and flow–drag-dependent damping (ζ_{fd}) were estimated by Rogers *et al.* (1984). The viscous damping is

$$\zeta_v = \left(\frac{\pi}{\sqrt{8}}\right)\left(\frac{\rho D}{m + m_a}\right)\left(\frac{2v}{\pi f D^2}\right)\left(D\sqrt{\frac{2\pi f}{v}}\right)\left[\frac{1 + (D/D_e)^3}{(1 - (D/D_e)^2)^2}\right], \tag{5}$$

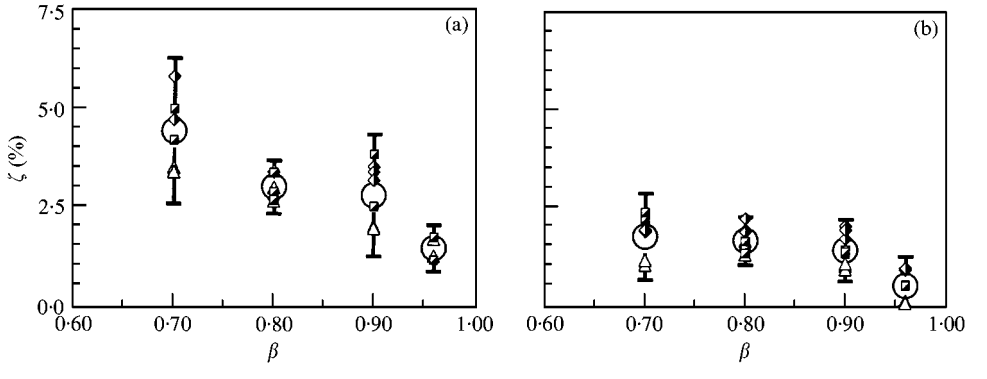

Figure 6. Damping versus β for the horizontal array; (a) drag and (b) lift, for tube: ◪ S2;△, S16 and ◆, S29. The large circular symbol indicates average damping at corresponding void fraction.

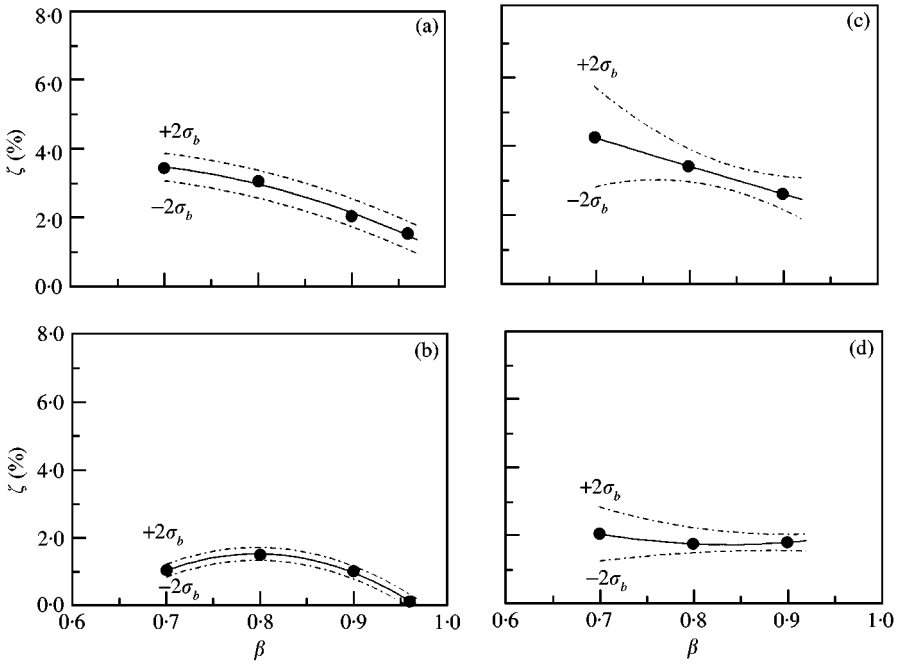

Figure 7. Tube S16 average damping variation with β at $P = 5{\cdot}8$ MPa for (a, b) horizontal array, (c, d) inclined array. (a, c) Show drag-direction damping, while (b, d) show lift-direction results.

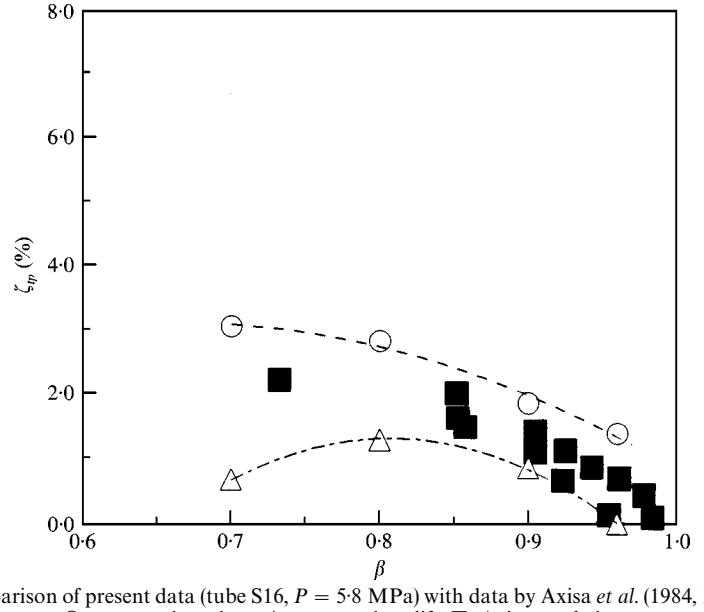

Figure 8. Comparison of present data (tube S16, $P = 5{\cdot}8$ MPa) with data by Axisa *et al.* (1984, 1985, 1986, 1988): ○, present data drag; △, present data lift; ■, Axisa *et al.* data.

where the equivalent two-phase viscosity $v = v_l / [1 + \beta(v_l/v_g - 1)]$, v_l and v_g being the respective liquid- and gas-phase viscosities, and $D/D_e = (1{\cdot}07 + 0{\cdot}56\mathrm{P}/D)P/D$, D_e being the hydraulic diameter. The drag-dependent damping is;

$$\zeta_{fd} \approx \frac{\rho U D C_D}{8\pi f(m + m_a)}, \quad C_D \approx 0{\cdot}2. \tag{6}$$

The data by Axisa *et al.* falls in a band between the lift and drag damping data from the present work, as seen in Figure 8.

5. ADDED MASS

In addition to the damping, the fluid added mass could also be determined. The added mass (m_a) was derived from the relative change in tube natural frequency. It is given by

$$m_a = m_s((f_s/f)^2 - 1). \tag{7}$$

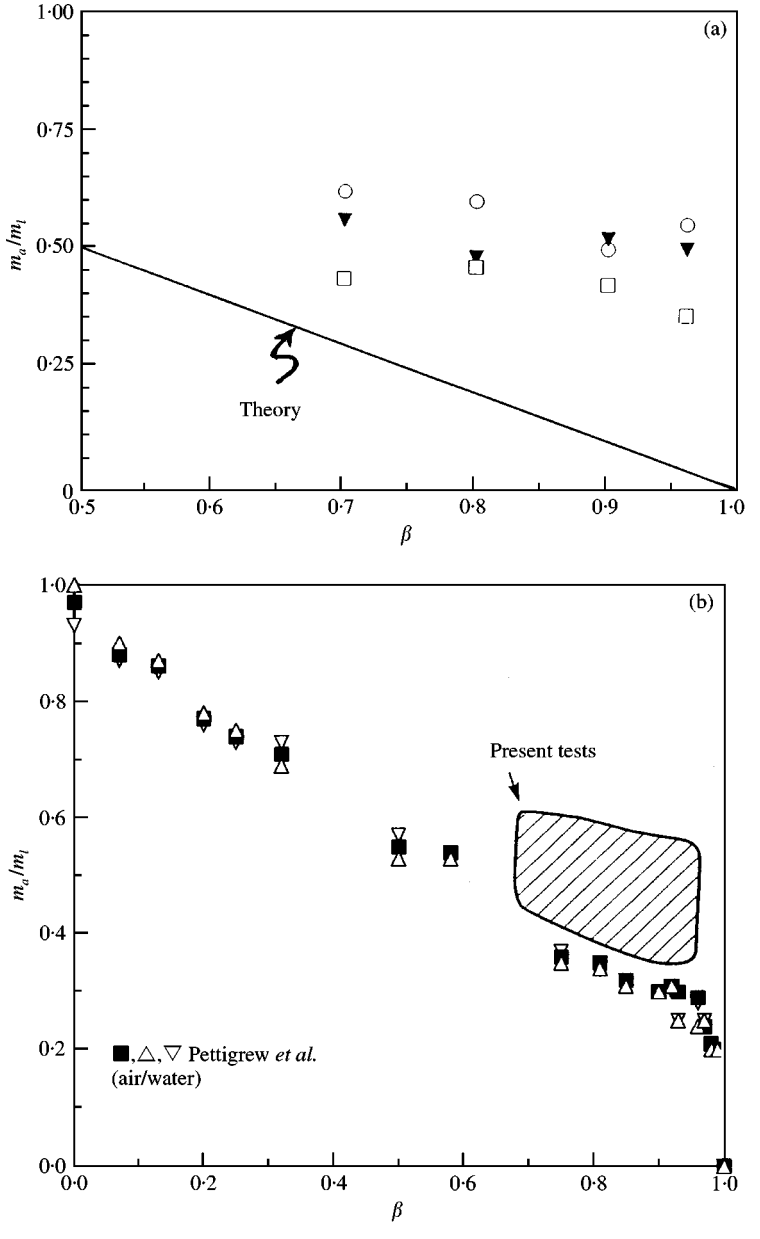

Figure 9. Added mass variation with β for (a) present data (□, S2; ▼, S16; ○, S29), $P = 5{\cdot}8$ MPa, and (b) comparison with data from Pettigrew *et al.* (1989).

In equation (7), m_s is the structural mass, and f_s the in-air frequency. The variation of m_a with β is shown in Figure 9(a) for tube S16. In the ratio m_a/m_l in the figure, m_l is the added mass in liquid (at the appropriate pressure). On average lift and drag direction added mass values are about equal. The data are compared to m_a^{th}/m_l, where the theoretical added mass (m_a^{th}) is calculated using the following model by Fritz (1972):

$$m_a^{\text{th}} = \frac{\pi}{4}\rho D^2 \left(\frac{(D_e/D)^2 + 1}{(D_e/D)^2 - 1}\right), \tag{8}$$

in which ρ_{tp} is the homogeneous two-phase density and D_e the hydraulic diameter. Agreement is poor. Figure 9(b) shows the comparison with the air–water data from Pettigrew *et al.* (1989). The added mass is slightly higher for steam–water for $\beta = 0{\cdot}70$–$0{\cdot}80$. A single-component mixture might be expected to result in higher added mass due to local phase transition.

6. CONCLUDING REMARKS

Two-phase flow-induced damping is highest in the drag direction, being approximately double that in the lift direction. Two-phase flow damping shows the typical parabolic-like drop with void fraction at $P = 5{\cdot}8$ MPa. The centrally located row-16 tube showed the lowest damping level. Damping levels at inlet and exit (rows 2 and 29) were approximately the same.

An inclination of the tubes relative to the flow resulted in slightly higher damping, compared to an orientation normal to the flow.

At a fixed flow velocity, damping in the lift direction decreased with ambient pressure and temperature. The effect of pressure is less clearly defined for the drag direction.

The variation of total damping with flow velocity is a good indicator for the onset of fluidelastic instability. Damping decrease with pressure seems to be associated with flow structure changes. At 0·5 MPa, for example, significant turbulence excitation occurs, while much lower turbulence excitation is observed at 5·8 MPa.

Added mass is slightly higher in steam–water mixtures compared to air–water mixtures. This might be attributed to phase transition (condensation on the tube surface) in single component mixtures.

ACKNOWLEDGEMENTS

This work was jointly financed by Mitsubishi Heavy Industries and the five electric power companies operating PWRs in Japan (Kansai Electric, Shikoku Electric, Kyushu Electric, Hokkaido Electric and the Japan Atomic Power Company). The authors gratefully acknowledge the assistance of T. Ueno with the interpretation of the thermal–hydraulics data.

References

Axisa, F., Villard, B., Gibert, R. J., Hetsroni, G. & Sundheimer, P. 1984 Vibration of tube bundles subjected to air–water and steam–water cross-flow: preliminary results on fluidelastic instability. In *Proceedings of the International Symposium on Flow-Induced Vibration and Noise*; Vol. 2: *Flow-Induced Vibration of Cylinder Arrays in Cross-Flow*, pp. 269–284. New York, ASME.

Axisa, F., Boheas, M. A. & Villard, B. 1985 Vibration of tube bundles subjected to steam-water cross-flow: a comparative study of square and triangular arrays. Paper B1/2, *Eighth International Conference on Structural Mechanics in Reactor Technology*, Brussels, Belgium.

AXISA, F., VILLARD, B. & SUNDHEIMER, P. 1986 Flow-induced vibration of steam generator tubes. *Electric Power Research Institute Report EPRI-NP*4559.

AXISA, F., WULLSCHLEGER, M., VILLARD, B. & TAYLOR, C. 1988 Two-phase cross-flow damping in tube arrays. In *Damping PVP-1998*, PVP-Vol-133. New York, ASME.

CARLUCCI, L. N. 1980 Damping and hydrodynamic mass of a cylinder in simulated two-phase flow. *ASME Journal of Mechanical Design* **102,** 597–602.

CARLUCCI, L. N. & BROWN, J. D. 1983 Experimental studies of damping and hydrodynamic mass of a cylinder in confined two-phase flow. *ASME Journal of Vibration, Acoustics, Stress, and Reliability in Design* **105,** 83–89.

COLLIER, J. G. 1981 *Convection, Boiling and Condensation.* NewYork: McGraw-Hill.

FRITZ, R. J. 1972 The effects of liquids on the dynamic motions of immersed solids. *ASME Journal of Engineering for Industry* **95,** 167–173.

HARA, F. 1993 A review of damping of two-phase flows. In *Seismic Engineering*, PVP Vol. 256–2. New York: ASME.

HARA, F. & KOHGO, O. 1986 Numerical approach to added mass and damping of a vibrating cylinder in a two-phase bubble fluid. In *Proceedings of the International Conference on Computational Mechanics*, Vol. 7, pp. 255–260, Tokyo, Japan.

HIROTA, K., NAKAMURA, T., MUREITHI, N. W., KASAHARA, J., KUSAKABE, T. & TAKAMATSU, H. 2002 Dynamics of an inline tube array subjected to steam–water cross-flow. Part III: fluidelastic instability tests and comparison with theory. *Journal of Fluids and Structures* **16,** 153–173.

HIROTA, K., NAKAMURA, T., MUREITHI, N. W., KASAHARA, J., KUSAKABE, T. & TAKAMATSU, H. 1996 Dynamics of an inline tube array in steam–water flow. Part III: fluidelastic instability tests and comparison with theory. In *Flow-Induced Vibration 1996* (ed. M. J. Pettigrew) , PVP Vol. 328, pp. 123–134. New York: ASME.

MUREITHI, N. W., NAKAMURA, T., HIROTA, K., FUJITA, K. & TAKAMATSU, H. 1995 Evaluation methodology of structural and flow induced damping of steam generator tubes. In *Proceedings of the Third JSME/ASME Joint International Conference on Nuclear Engineering* (*ICONE 3*), Vol. 1, pp. 613–618, Kyoto, Japan.

MUREITHI, N. W., NAKAMURA, T., HIROTA, K., MURATA, M., UTSUMI, S., KUSAKABE, T. & TAKAMATSU, H. 1996 Dynamics of an inline tube array in steam-water flow: Part II: unsteady fluid forces. In *Flow-Induced Vibration 1996* (ed. M. J. Pettigrew), PVP Vol. 328, pp. 111–121. New York: ASME.

MUREITHI, N. W., NAKAMURA, T., HIROTA, K., MURATA, M., UTSUMI, S., KUSAKABE, T. & TAKAMATSU, H. 2002 Dynamics of an inline tube array subjected to steam-water cross-flow. Part II: unsteady fluid forces. *Journal of Fluids and Structures* **16,** 137–152.

NAKAMURA, T., FUJITA, K., KAWANISHI, K., YAMAGUCHI, N. & TSUGE, A. 1995 Study on the vibrational characteristics of a tube array caused by two-phase flow. Part II: fluidelastic vibration. *Journal of Fluids and Structures* **9,** 539–562.

NAKAMURA, T., MUREITHI, N. W., HIROTA, K., MURATA, M., WATANABE, Y., KUSAKABE, T. & TAKAMATSU, H. 1996 Dynamics of an inline tube array in steam–water flow. Part I: damping and added mass. In *Flow-Induced Vibration* 1996 (ed. M. J. Pettigrew), PVP Vol. 328, pp. 103–110. New York: ASME.

PETTIGREW, M. J. & GORMAN, D. J. 1981 Vibration of heat exchanger tube bundles in liquid and two-phase cross-flow. In *Flow Induced Vibration Design Guidelines*, PVP Vol. 52, pp. 89–110. New York: ASME.

PETTIGREW, M. J., TROMP, J. H. & MASTORAKOS, J. 1985 Vibration of tube bundles subjected to two-phase cross-flow. *ASME Journal of Pressure Vessel Technology* **107,** 335–343.

PETTIGREW, M. J., TAYLOR, C. E. & KIM, B. S. 1989 Vibration of tube bundles in two-phase cross flow. Part I: hydrodynamic mass and damping. *ASME Journal of Pressure Vessel Technology* **111**, 466–477.

PETTIGREW, M. J. & KNOWLES, G. D. 1992 Some aspects of heat exchanger tube damping in two-phase mixtures. In *Proceedings of the International Symposium on Flow-Induced Vibration and Noise*; Vol. 1: *FSI/FIV in Cylinder Arrays in Cross-Flow*, pp. 141–160. New York: ASME

ROGERS, R. J., TAYLOR, C. & PETTIGREW, M. J. 1984 Fluid effects on multi-span heat exchanger tube vibration. In *Proceedings of the ASME-PVP Conference*, San Antonio, TX.

ULBRICH, R. & MEWES, D. 1994 Vertical, upward gas–liquid two-phase flow across a tube bundle. *International Journal of Multiphase Flow* **20,** 249–272.

APPENDIX A

Flow patterns for flow across tube arrays are as yet not fully identified. For air–water flow, however, some recent excellent work by Ulbrich and Mewes (1994) has made it possible to determine transition boundaries with reasonable certainty. Freon two-phase flow data were also considered. Their proposed flow pattern map is based on superficial gas and liquid velocities.

In the present tests superficial fluid velocities were identical for $P = 0{\cdot}5$, $3{\cdot}0$ and $5{\cdot}8$ MPa tests; for $P = 0{\cdot}5$ MPa, wider velocity ranges were tested. Besides flow velocities, flow pattern transitions are associated mainly with changes in fluid density and associated momentum due to ambient pressure changes. Figure A.1 shows the present tests conditions superimposed on a map from Collier (1981). While this map is intended for flow transition in vertical axial flow, it gives an idea of the effect of pressure change on flow pattern. At $5{\cdot}8$ MPa, the flow pattern falls in the churn-annular regime. For $0{\cdot}5$ MPa, mainly churn flow is predicted; however, the test conditions fall close to the intermittent slug flow boundary.

Simultaneously with the vibration tests discussed in this paper, several thermal–hydraulic measurements were also made. With regard to flow pattern within the array, the most relevant quantity is the local instantaneous void fraction measurement. One of the measurement locations was immediately downstream of tube S16 (in the gap between rows 18 and 19). A void sensor probe monitored the relative duration of gas and fluid phases at a point. The void probe is shown schematically in Figure A.2. The presence of water at the probe tip completes the circuit, resulting in a voltage $V = 1{\cdot}0$ V (high level). Vapour, having low

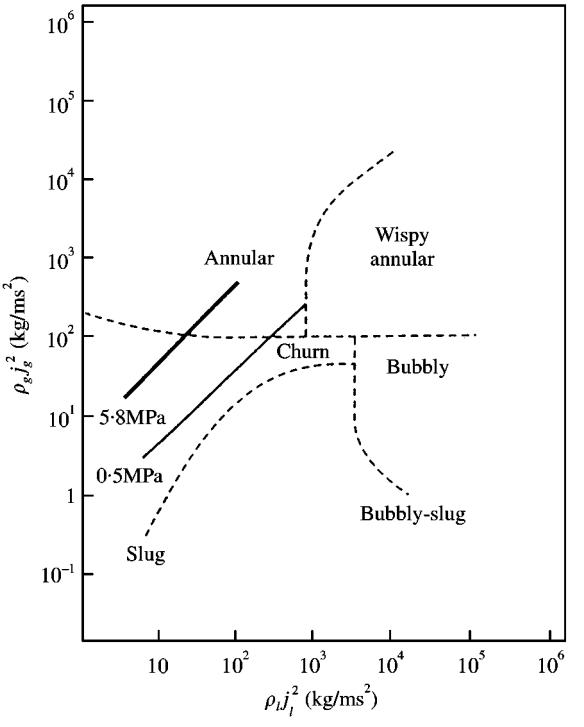

Figure A.1. Flow conditions for present tests superimposed on a map taken from Collier (1981).

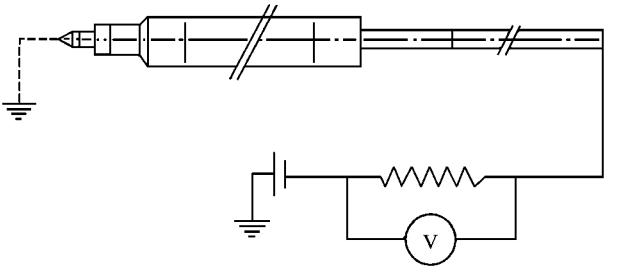

Figure A.2. Schematic of void sensing probe.

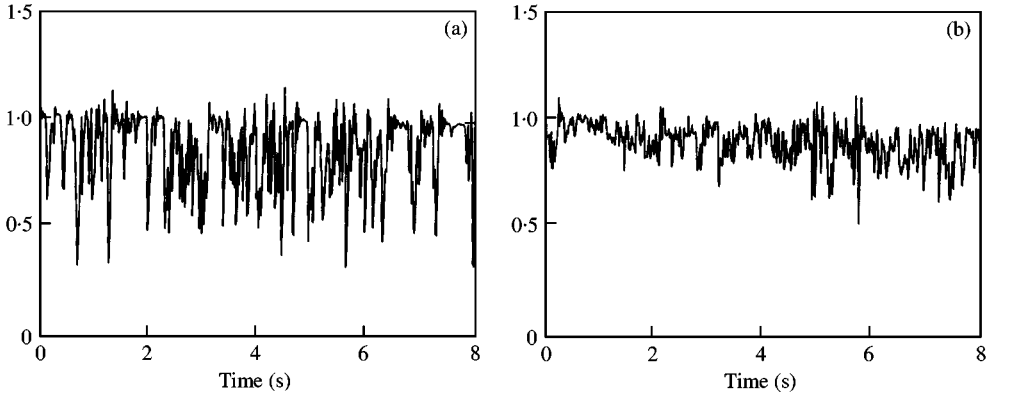

Figure A.3. Void sensor output voltage signal at superficial velocities $j_l = 0{\cdot}10$ m/s and $j_g = 0{\cdot}9$ m/s for (a) $P = 0{\cdot}5$ MPa and (b) $P = 5{\cdot}8$ MPa.

conductivity, results in a voltage $V = 0{\cdot}5$ V (low level). Intermediate values reflect the presence of a mixture of liquid and vapour. In Figure A.3 void sensor voltage outputs are shown for $P = 0{\cdot}5$ and $5{\cdot}8$ MPa. Clear transitions in the local fluid phase are evident for $P = 0{\cdot}5$ MPa. The slight overshooting and undershooting in the signal is related to the sensor electronics; the signal, however, settles down if the new fluid phase persists. The flow is clearly intermittent and with significant slugging for $0{\cdot}5$ MPa. On the other hand, for $P = 5{\cdot}8$ MPa there are no clear transitions indicating the local flow pattern to be homogeneous, froth/churn flow. This was also the case for $P = 3{\cdot}0$ MPa.